www.ietdl.org

Published in IET Renewable Power Generation
Received on 10th March 2013
Revised on 6th June 2013
Accepted on 2nd July 2013
doi: 10.1049/iet-rpg.2013.0078

ISSN 1752-1416

Model predictive control of inverters for both islanded and grid-connected operations in renewable power generations

Jiefeng Hu, Jianguo Zhu, David G. Dorrell

Faculty of Engineering and Information Technology, University of Technology, Sydney, Australia
E-mail: Jiefeng.Hu@uts.edu.au

Abstract: As the penetration of renewable power generation units connected to the grid increases, high power quality and flexible power regulation have raised much concern. This study proposes a competitive model predictive control strategy for inverters in renewable power generation applications. The controller uses the system model to predict the system behaviour in each sampling interval for each voltage vector, and the most appropriate vector is then chosen according to an optimisation criterion. In islanded mode, the control objectives of the cost function are the α and β components of the voltage so that stable voltage for the local loads can be established. In addition, a fast re-synchronisation scheme is introduced to achieve smooth grid connection. After connected to the grid, a new prediction scheme is developed to fulfill flexible active and reactive power regulation. Furthermore, a switching frequency reduction scheme is presented to reduce switching losses, which are especially significant when considering efficiency for renewable power generations. The effectiveness of the proposed control strategy was tested by simulation using MATLAB/Simulink and experimentally validated on a laboratory prototype.

1 Introduction

Owing to the rapid depletion of fossil fuels and the government policy of reducing carbon dioxide emissions, more and more distributed generation (DG) plants are being developed, especially plants that exploit renewable energy such as wind turbines and photovoltaic (PV) plants. These are usually connected to low-voltage distribution lines. As the penetration and capacities of DG units increase, the power converters associated with these plants are required to operate more efficiently and effectively in order to maintain high power quality and dynamic stability [1–3]. To fulfill these requirements, advanced control techniques are essential.

In a DG system, there are generally two operation modes: the islanded mode and the grid-connected mode. In the islanded mode, the DG sources and the local loads form an isolated small power system, where the loads are totally powered by the DG units. In this case, the inverters should be able to provide a stable and high quality voltage for the local loads. In addition, these DG units should be able to achieve grid synchronisation and re-connection. A basic requirement here is that the transfer process should be as fast as possible, and not have any negative effect on the utility grid or the DG itself [4, 5]. After grid connection, the DGs should flexibly regulate active and reactive powers injected into the grid. They could also be used to provide voltage support and power quality improvement at the low voltage distribution level [6, 7].

Although many control methods have been developed to control the inverters connected to a distributed generation system, these methods mainly focus on one specific operation mode; either islanded operation or grid-connected operation. In the last decade, some studies have investigated the control of inverters in islanded operation with a particular focus on uninterruptible power supply (UPS) applications. These include deadbeat control [8, 9], adaptive control [10], multiloop feedback control [11, 12] and others. However, these schemes use the output voltage and current with outer and inner control loops, thus proportional-integral (PI) regulators and pulse-width modulation (PWM) modulators are required, and tuning effort is needed in practical implementation. Recently a control approach based on model predictive control (MPC) was proposed, there is no need for internal current-control loops or modulators, and the scheme is easy to implement [13].

Attention has also been paid to the control of grid-connected inverters. Direct power control (DPC), derived from direct torque control of an AC machine, has become one of the most popular control strategies for grid-connected inverters because of its simplicity and excellent dynamic response. However, high power ripple is the main drawback of the conventional switching-table-based DPC (STDPC), leading to distorted line currents [14]. Recently some improved DPC methods have been developed for better performance [15–17]. Even more recently predictive control techniques have become an attractive alternative for the control of power converters.

Among these, MPC has attracted much attention, predominantly because it has a flexible control scheme that allows the easy inclusion of system constraints and non-linearities. In this control, a model is used to predict the system behaviour, and a cost function is employed as a criterion to select the optimal switching states. The control objectives of MPC can vary considerably according to the application. For example, the control objective is the inverter output voltage for a UPS system in [13]. In other applications, the objectives are the active and reactive powers in [18, 19] for a rectifier; and the currents in [20–22] for an inverter connected to an electrical machine or other electric load. Nevertheless, the MPC strategy for a grid-connected inverter is seldom mentioned in the literature.

This paper proposes a MPC strategy for an inverter utilised in a renewable power generation system which is sufficiently flexible to achieve islanded operation, grid synchronisation, and grid-connected operation. By changing the cost function correctly this control strategy can be employed to achieve stable voltage, fast and smooth grid synchronisation, and flexible active and reactive power regulation. This control strategy is simple and easy to implement. No PI regulators and PWM modulators are required; synchronous coordinate transformation is also eliminated, presenting excellent steady state and dynamic performance.

2 System modelling

A three-phase two-level inverter-based renewable power generation system is considered in this paper, as shown in Fig. 1. The inverter output voltage $\boldsymbol{V}_i$ can be controlled to eight vectors and determined by the switching states, which can be expressed in complex space vectors as

$$\boldsymbol{V}_i = \begin{cases} \frac{2}{3} V_{\mathrm{dc}} \mathrm{e}^{\mathrm{j}(i-1)\frac{\pi}{3}} & (i = 1 \cdots 6) \\ 0 & (i = 0, 7) \end{cases} \tag{1}$$

2.1 Model of islanded pperation

In islanded operation, the static transfer switch S_1 is OFF while the bypass switch S_2 is ON. The renewable power generation system supplies the power to the local load. In this scenario, the dynamic behaviour of the capacitor in the LC filter can be expressed as

$$C\frac{\mathrm{d}\boldsymbol{V}_c}{\mathrm{d}t} = \boldsymbol{i}_f - \boldsymbol{i}_{\mathrm{L}} \tag{2}$$

where C is the filter capacitance, $\boldsymbol{V}_{\mathrm{c}}$ is the capacitor voltage vector, $\boldsymbol{i}_f$ is the inductor current vector, and $\boldsymbol{i}_{\mathrm{L}}$ is the load current vector ($\boldsymbol{i}_{\mathrm{o}} = \boldsymbol{i}_{\mathrm{L}}$). The voltage equation of the inductor in the LC filter can be described by

$$\boldsymbol{V}_i = \boldsymbol{V}_c + \boldsymbol{i}_f R + L\frac{\mathrm{d}\boldsymbol{i}_f}{\mathrm{d}t} \tag{3}$$

where R and L are the filter resistance and inductance, respectively.

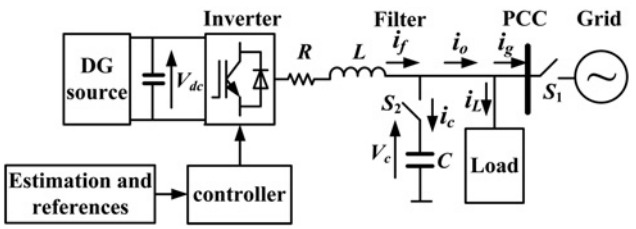

Fig. 1 *One-phase model of inverter-based renewable power generation system*

2.2 Model of grid-connected operation

In grid-connected operation, the static transfer switch S_1 is ON while the bypass switch S_2 is OFF. The inverter is connected to the grid through the line inductor, and the renewable power generation system supplies the power to the local load together with the grid. The excess power generated will be injected to the grid. In this case, the mathematical model of the system can be expressed as

$$\boldsymbol{i}_f = \boldsymbol{i}_o \tag{4}$$

$$\boldsymbol{i}_{\mathrm{o}} = \boldsymbol{i}_{\mathrm{L}} + \boldsymbol{i}_{\mathrm{g}} \tag{5}$$

$$\boldsymbol{V}_i = \boldsymbol{V}_{\mathrm{g}} + \boldsymbol{i}_{\mathrm{o}} R + L\frac{\mathrm{d}\boldsymbol{i}_{\mathrm{o}}}{\mathrm{d}t} \tag{6}$$

where $\boldsymbol{V}_{\mathrm{g}}$ is the grid voltage vector, $\boldsymbol{i}_{\mathrm{g}}$ is the current vector injected into the grid and $\boldsymbol{i}_{\mathrm{o}}$ is the inverter output current vector (after the LC filter), as depicted in Fig. 1. The inverter instantaneous output active and reactive powers are

$$P = \frac{3}{2}\mathrm{Re}\left\{\boldsymbol{V}_{\mathrm{g}}\boldsymbol{i}_{\mathrm{o}}^{*}\right\} = \frac{3}{2}\left(V_{\mathrm{g}\alpha} i_{\mathrm{o}\alpha} + V_{\mathrm{g}\beta} i_{\mathrm{o}\beta}\right) \tag{7}$$

$$Q = \frac{3}{2}\mathrm{Im}\left\{\boldsymbol{V}_{\mathrm{g}}\boldsymbol{i}_{\mathrm{o}}^{*}\right\} = \frac{3}{2}\left(V_{\mathrm{g}\beta} i_{\mathrm{o}\alpha} - V_{\mathrm{g}\alpha} i_{\mathrm{o}\beta}\right) \tag{8}$$

where * donates the complex conjugate, $V_{\mathrm{g}\alpha}$ and $V_{\mathrm{g}\beta}$ are the real and imaginary components of $\boldsymbol{V}_{\mathrm{g}}$, while $i_{\mathrm{o}\alpha}$ and $i_{\mathrm{o}\beta}$ are the real and imaginary components of $\boldsymbol{i}_{\mathrm{o}}$. In other words, $\boldsymbol{V}_{\mathrm{g}} = V_{\mathrm{g}\alpha} + jV_{\mathrm{g}\beta}$, $\boldsymbol{i}_{\mathrm{o}} = i_{\mathrm{o}\alpha} + ji_{\mathrm{o}\beta}$.

3 Voltage control in islanded mode

In the islanded mode, the aim of the MPC controller is to manage the inverter to establish a stable voltage for the local loads without power supply from the grid. With this goal, the MPC voltage controller predicts the future behaviour of the capacitor voltage $\boldsymbol{V}_{\mathrm{c}}$. Combining (2) and (3), the system model can be rewritten as a state-space system

$$\frac{\mathrm{d}\boldsymbol{x}}{\mathrm{d}t} = A\boldsymbol{x} + B\boldsymbol{V}_i + D\boldsymbol{i}_{\mathrm{L}} \tag{9}$$

where

$$\boldsymbol{x} = \begin{bmatrix} \boldsymbol{i}_f \\ \boldsymbol{V}_c \end{bmatrix}, \quad A = \begin{bmatrix} -R/L & -1/L \\ 1/C & 0 \end{bmatrix}, \quad B = \begin{bmatrix} 1/L \\ 0 \end{bmatrix}, \quad D = \begin{bmatrix} 0 \\ -1/C \end{bmatrix}$$

Since the sampling time T_s is very small, one can assume

$$e^{AT_s} = 1 + AT_s + \frac{(AT_s)^2}{2!} + \cdots + \frac{(AT_s)^n}{n!} \simeq 1 + AT_s \quad (10)$$

Therefore the discrete-time model of the LC filter for a sampling time T_s can be expressed by Cortés *et al.* [13]

$$\boldsymbol{x}(k+1) = A_a \boldsymbol{x}(k) + B_b \boldsymbol{V}_i(k) + D_d \boldsymbol{i}_L(k) \quad (11)$$

where

$$A_a = e^{AT_s}, \quad B_b = \int_0^{T_s} e^{A\tau} d\tau, \quad D_d = \int_0^{T_s} e^{A\tau} D d\tau$$

Consequently, the capacitor voltage at $(k+1)$th instant can be predicted:

$$\boldsymbol{V}_c(k+1) = \boldsymbol{V}_c(k) + e^{T_s/C} \boldsymbol{i}_f(k) + \frac{C\left(e^{T_s/C} - 1\right)}{L} \boldsymbol{V}_i(k) - \frac{T_s}{C} \boldsymbol{i}_L(k) \quad (12)$$

To control the capacitor voltage, the cost function J_V can be defined so that

$$J_V = \left(V_{c\alpha}^{\text{ref}} - V_{c\alpha}^{k+1}\right)^2 + \left(V_{c\beta}^{\text{ref}} - V_{c\beta}^{k+1}\right)^2 \quad (13)$$

where $V_{c\alpha}^{k+1}$ and $V_{c\beta}^{k+1}$ are the real and imaginary components of the predicted capacitor voltage vector, respectively. In other words, $\boldsymbol{V}_c(k+1) = V_{c\alpha}^{k+1} + jV_{c\beta}^{k+1}$. According to this cost function, the voltage vector that generates the least value of J_V will be applied during the next sampling period. The block diagram of the voltage control is illustrated in Fig. 2.

According to (13), the $\boldsymbol{V}_c$ can track its reference because the α and β components are tightly controlled. Based on this analysis, it is expected that grid synchronisation can be achieved by replacing the referenced voltage V_c^{ref} with the grid voltage $\boldsymbol{V}_g$, as illustrated in Fig. 2. Therefore the cost function can be revised:

$$J_V = \left(V_{g\alpha} - V_{c\alpha}^{k+1}\right)^2 + \left(V_{g\beta} - V_{c\beta}^{k+1}\right)^2 \quad (14)$$

Using (14), the capacitor voltage can closely track the grid voltage in terms of phase angle, amplitude and frequency. When the grid synchronisation process is completed, the renewable power generation system is ready for grid connection.

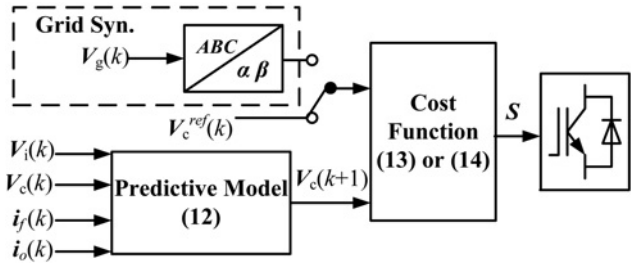

Fig. 2 *Block diagram of voltage control*

4 Flexible power regulation in grid-connected mode

Once a DG unit is connected to the main grid, flexible active and reactive power regulation must be achieved to help improve system stability and power quality [23, 24]. Therefore the control the objectives of MPC become the active and reactive powers. Once the static transfer switch S_1 is closed, the bypass switch S_2 is switched OFF. The inverter is then supplying active and reactive power to the local load and the grid through the L filter. According to (7) and (8), the inverter active and reactive power derivatives can be calculated from

$$\frac{dP}{dt} = \frac{3}{2}\left(\frac{dV_{g\alpha}}{dt} i_{o\alpha} + V_{g\alpha}\frac{di_{o\alpha}}{dt} + \frac{dV_{g\beta}}{dt} i_{o\beta} + V_{g\beta}\frac{di_{o\beta}}{dt}\right) \quad (15)$$

$$\frac{dQ}{dt} = \frac{3}{2}\left(\frac{dV_{g\beta}}{dt} i_{o\alpha} + V_{g\beta}\frac{di_{o\alpha}}{dt} - \frac{dV_{g\alpha}}{dt} i_{o\beta} - V_{g\alpha}\frac{di_{o\beta}}{dt}\right) \quad (16)$$

If we consider sinusoidal and balanced line voltage, one can obtain

$$\boldsymbol{V}_g = V_{g\alpha} + jV_{g\beta} = |\boldsymbol{V}_g| e^{j\omega t} = |\boldsymbol{V}_g| \cos \omega t + j|\boldsymbol{V}_g| \sin \omega t \quad (17)$$

$$\frac{dV_{g\alpha}}{dt} = \frac{d\left(|\boldsymbol{V}_g| \cos \omega t\right)}{dt} = -\omega |\boldsymbol{V}_g| \sin \omega t = -\omega V_{g\beta} \quad (18)$$

$$\frac{dV_{g\beta}}{dt} = \frac{d\left(|\boldsymbol{V}_g| \sin \omega t\right)}{dt} = \omega |\boldsymbol{V}_g| \cos \omega t = \omega V_{g\alpha} \quad (19)$$

where ω is the grid voltage frequency in rad/s. The inverter output active and reactive power derivations can then be obtained by substituting (6), (18) and (19) into (15) and (16) so that

$$\frac{dP}{dt} = \frac{3}{2}\left[-\omega V_{g\beta} i_{o\alpha} + \frac{V_{g\alpha}}{L}\left(V_{i\alpha} - V_{g\alpha} - i_{o\alpha}R\right) + \omega V_{g\alpha} i_{o\beta} + V_{g\beta}\left(V_{i\beta} - V_{g\beta} - i_{o\beta}R\right)\right] \quad (20)$$

$$\frac{dQ}{dt} = \frac{3}{2}\left[\omega V_{g\alpha} i_{o\alpha} + \frac{V_{g\beta}}{L}\left(V_{i\alpha} - V_{g\alpha} - i_{o\alpha}R\right) + \omega V_{g\beta} i_{o\beta} - V_{g\alpha}\left(V_{i\beta} - V_{g\beta} - i_{o\beta}R\right)\right] \quad (21)$$

By considering (7), (8), $\boldsymbol{V}_g \boldsymbol{V}_i^* = \left(\boldsymbol{V}_{g\alpha}\boldsymbol{V}_{i\alpha} + \boldsymbol{V}_{g\beta}\boldsymbol{V}_{i\beta}\right) + j\left(\boldsymbol{V}_{g\beta}\boldsymbol{V}_{i\alpha} - \boldsymbol{V}_{g\alpha}\boldsymbol{V}_{i\beta}\right)$, and $\left|\boldsymbol{V}_g\right|^2 = \boldsymbol{V}_{g\alpha}^2 + \boldsymbol{V}_{g\beta}^2$, (20) and (21) can be rewritten as

$$\frac{dP}{dt} = -\frac{R}{L}P - \omega Q + \frac{3}{2L}\left(\text{Re}\left(\boldsymbol{V}_g \boldsymbol{V}_i^*\right) - \left|\boldsymbol{V}_g\right|^2\right) \quad (22)$$

$$\frac{dQ}{dt} = \omega P - \frac{R}{L}Q + \frac{3}{2L}\text{Im}\left(\boldsymbol{V}_g \boldsymbol{V}_i^*\right) \quad (23)$$

where once again * donates the complex conjugate. Therefore the active and reactive power at the end of the sampling

doi: 10.1049/iet-rpg.2013.0078

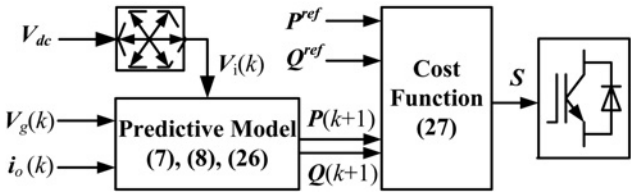

Fig. 3 *Block diagram of flexible power regulation*

period T_s can be predicted from

$$P^{k+1} = T_s\left[-\frac{R}{L}P - \omega Q + \frac{3}{2L}\left(\mathrm{Re}\left(\boldsymbol{V}_g \boldsymbol{V}_i^*\right) - \left|\boldsymbol{V}_g\right|^2\right)\right] + P^k \tag{24}$$

$$Q^{k+1} = T_s\left[\omega P - \frac{R}{L}Q + \frac{3}{2L}\mathrm{Im}\left(\boldsymbol{V}_g \boldsymbol{V}_i^*\right)\right] + Q^k \tag{25}$$

However, it can be seen that the power prediction using (24) and (25) would be very complicated, making implementation difficult. In this paper, a new and simple prediction scheme is developed. The discrete-time model of (6) can be expressed as

$$\boldsymbol{i}_o(k+1) = T_s\left(\boldsymbol{V}_i(k) - \boldsymbol{V}_g(k) - \boldsymbol{i}_o(k)R\right)/L + \boldsymbol{i}_o(k) \tag{26}$$

Assuming the grid voltage is constant during the sampling period, $P(k+1)$ and $Q(k+1)$ can be calculated by substituting (26) into (7) and (8). This prediction scheme is more straightforward than (24) and (25) where power derivatives are used, thus reducing the computational burden. This is quite useful for MPC because calculating the cost function can be very time consuming for a hardware processor, especially if several constraints are included in the cost function while high sampling frequency is required.

After the power is predicted, the next step is to evaluate the effects of each voltage vector on the active and reactive powers and to select the one which produces the least power ripple according to a specific cost function. In this paper, the cost function is defined by

$$J_P = \left(P^{\mathrm{ref}} - P^{k+1}\right)^2 + \left(Q^{\mathrm{ref}} - Q^{k+1}\right)^2 \tag{27}$$

The block diagram of grid-connected operation is as shown in Fig. 3.

5 Switching frequency reduction

When the renewable power generation system injects power into the grid, power conversion efficiency is a significant concern. Since large capacity distributed power generation with high voltage levels is likely to increase in popularity, switching frequency reduction has attracted attention. This is because the switching loss can be reduced by use of lower switching frequency in the converter. With lower the switching frequency, there can be less power loss with no system performance deterioration; that is, higher efficiency can be obtained. Here, in order to reduce the switching

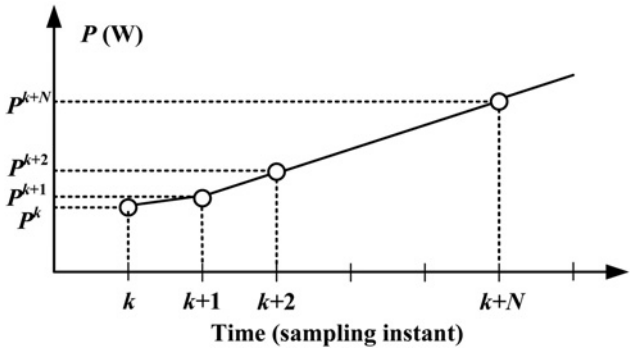

Fig. 4 *Active power trajectories and switching position with N-step prediction*

frequency, the expression of cost function (27) is revised to

$$J_P = \left(\left(P^{\mathrm{ref}} - P^{k+1}\right)^2 + \left(Q^{\mathrm{ref}} - Q^{k+1}\right)^2\right) + \lambda_2\left(\sum_{i=a,b,c}\left|D_i^{k+1} - D_i^k\right|\right) \tag{28}$$

where D_i^{k+1} and D_i^k represent the switching state of the rectifier leg i ($i = a, b, c$) at the current control period and the next control period, respectively. $D_i = 0$ or 1, 0 means the upper transistor is OFF and the lower one is ON, 1 indicates the inverse switching state, λ_2 is the weighting factor. The first term in (28) reduces the power ripple and helps track the reference while the second term contributes to the objective of switching frequency reduction. A large value of the weighting factor λ_2 implies greater priority to the latter objective. Therefore by defining the cost function as (28), the switching frequency can be taken into account. Bear in mind that eight possible vectors should be evaluated in (28) for switching frequency reduction, although only seven vectors are needed for (27) because the effects of $\boldsymbol{V}_0$ and $\boldsymbol{V}_7$ are the same when the reduction of the switching frequency is not considered.

Note that if λ_2 is too large; that is, switching frequency reduction is more aggressive than necessary, the system stability will deteriorate, resulting in excessively large currents and power ripple. In order to reduce the switching frequency without system performance deterioration, an N-step horizontal prediction for system stability improvement has been developed. The inverter output power at the $(k+N)$th instant is predicted from the value at the $(k+1)$th and $(k+2)$th instants using linear extrapolations. To visualise this prediction theory, Fig. 4 depicts an example of the active power trajectory and the switching position with N-step prediction. The active and

Table 1 System parameters

Line resistance R	0.51 Ω
filter inductance L	4.8 mH
filter capacitor C	36 uF
line-line voltage V_g	120 V (rms)
voltage frequency f	50 Hz
DC source voltage V_{dc}	250 V
sampling period T_s	50 μs
local load R_L	50 Ω
weighting factor λ_2	75
weighting factor λ_3	0.16

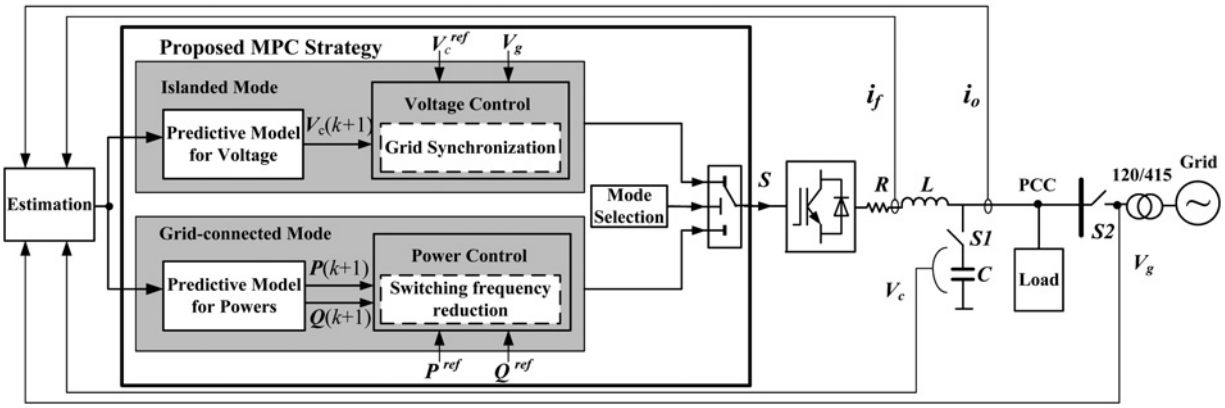

Fig. 5 *Block diagram of the proposed MPC strategy for renewable power generations*

reactive powers at the $(k+N)$th instant can be predicted from

$$P^{k+N} = P^{k+1} + (N-1)\left(P^{k+2} - P^{k+1}\right) \tag{29}$$

$$Q^{k+N} = Q^{k+1} + (N-1)\left(Q^{k+2} - Q^{k+1}\right) \tag{30}$$

where P^{k+1}, Q^{k+1}, P^{k+2} and Q^{k+2} can be obtained using the method presented in Section 4. In this paper, $N=5$. Consequently, the cost function (28) can be further revised to (see (31))

where λ_3 is the weighting factor of the component in charge of system stability. Using linear extrapolation for the approximate prediction, where the coincidence point N is larger than 2, this is feasible, especially when the sampling period is short. This will be validated in the simulation and experimental results in the next sections.

6 Simulation results

The proposed control strategy was tested in simulation using MATLAB/Simulink. The system parameters are listed in Table 1. A constant 250 V DC source is used to simulate the renewable energy source output. The control system starts to operate at 0.02 s, the grid synchronisation begins at 0.1 s and the DG system is connected to the grid at 0.15 s with $P^{\text{ref}}=0$ W and $Q^{\text{ref}}=0$ VAr initially. A block diagram of the whole proposed control strategy is shown Fig. 5. The basic operation of the proposed renewable power system is as follows. When a utility grid fault occurs, the renewable power system should be isolated from the grid. In this case, the grid is unavailable and a stable and high quality voltage must be established for the local load within the renewable power system. Therefore the voltage control cost function (13) should be used. After clearance of the grid fault, the renewable power system should be re-connected to the grid, which can be achieved simply by using the grid voltage as the reference; that is, the grid synchronisation cost function (14) should be utilised. After grid connection, the utility grid voltage is available to the local load. In this case, obviously the renewable power system should be able to supply active and reactive powers to the utility grid flexibly and efficiently. Consequently, the cost function (31) for flexible power regulation with switching frequency reduction should be employed.

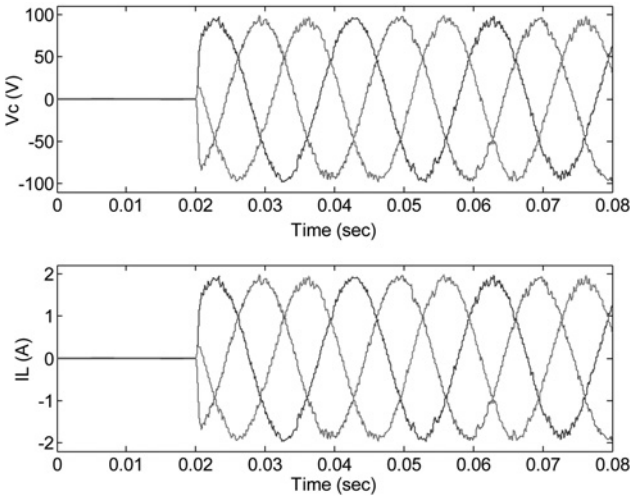

Fig. 6 *Simulation results of capacitor voltage and load current*

6.1 Islanded operation

Fig. 6 shows the capacitor voltage ($\boldsymbol{V}_{\text{c}}$) and load current ($\boldsymbol{i}_{\text{L}}$) in islanded operation. It can be seen that a stable voltage is established very quickly, and this is sinusoidal with low distortion (total harmonic distortion (THD) = 2.54%). A zoom-in of the phase A voltage V_{ca} and its spectrum are shown in Fig. 7.

6.2 Grid Synchronisation

The grid synchronisation process and grid connection are presented in Fig. 8. From top to bottom, the waveforms are: capacitor phase A voltage (V_{ca}), grid phase A voltage (V_{ga}), and inverter output currents ($\boldsymbol{i}_{\text{o}}$). It can be seen that the inverter output voltage can match the grid voltage in less than 1 ms once the grid synchronisation algorithm starts to

$$J_P = \left(\left(P^{\text{ref}} - P^{k+1}\right)^2 + \left(Q^{\text{ref}} - Q^{k+1}\right)^2\right) + \lambda_2\left(\sum_{i=a,b,c}\left|D_i^{k+1} - D_i^k\right|\right) + \lambda_3\left(\left|P^{\text{ref}} - P^{k+N}\right| + \left|Q^{\text{ref}} - Q^{k+N}\right|\right) \tag{31}$$

doi: 10.1049/iet-rpg.2013.0078

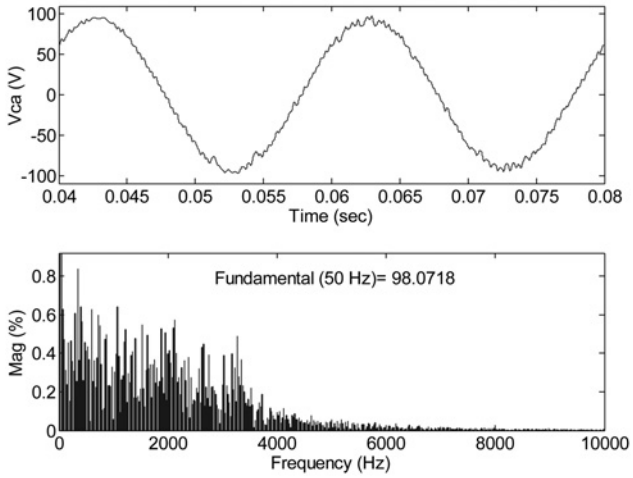

Fig. 7 *Spectra of capacitor voltage, THD = 2.54%*

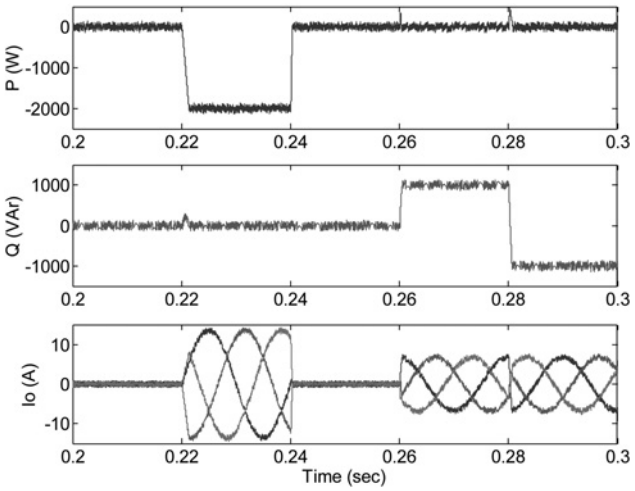

Fig. 9 *Simulation results of flexible power regulation*

operate. After the voltage is synchronised with the grid voltage, in terms of amplitude, frequency and phase angle, the renewable power generation system is connected to the grid through the static transfer switch. The capacitor of the LC filter is bypassed at 0.15 s. It can be observed that the grid connection is very smooth without obvious over-shoot current. It can also be noted that the P and Q references are set to zero during the grid connection process. After successful grid connection at 0.15 s, the inverter system can be controlled in order to output any active or reactive power within its capacity. Here, the inverter starts to output active power at 0.22 s, as illustrated in Fig. 9. Therefore the inverter output current $\boldsymbol{i}_o$ is zero between 0.15 s and 0.22 s because P and Q are controlled to be zero.

6.3 Flexible power regulation in grid-connected mode

Fig. 9 presents the power regulation performance. Initially the reactive power is set to 0 VAr while the active power is stepped from 0 to -2 kW at 0.22 s and backed to 0 W at 0.24 s. After that, the active power is kept at 0 W while the reactive is stepped to 1 kVar and then to -1 kVar. It can be seen that the proposed MPC strategy presents excellent dynamic response, tracking the references in less than 0.5 ms.

7 Experimental results

The proposed control strategy was further validated by experiment using a laboratory PV system setup, as shown in Fig. 10. It consists of the following devices: a three-phase Semikron intelligent insulated gate bipolar transistor power module as the inverter, an ABB DC power source, a three-phase LC filter, an over-current protection device and a three-phase isolated transformer to increase the inverter output voltage from 120 to 415 V from the main grid. A dSPACE DS1104 power PC (PPC)/digital signal processor (DSP) control board was employed in order to implement the real-time algorithm coding using C language for the control. The voltages and currents are sampled using ControlDesk, which is interfaced with the DS1104 and a PC at a rate of 20 kHz. The system parameters are the same as the simulation.

7.1 Islanded operation

In islanded operation, the static transfer switch S1 is OFF while the bypass switch S2 is ON, and the islanded mode is selected, as illustrated in Fig. 5. The experimental results of the islanded operation are shown in Fig. 11. From top to bottom, the curves shown in Fig. 11*a* are the capacitor voltage, load current and inductor current of the LC filter. It

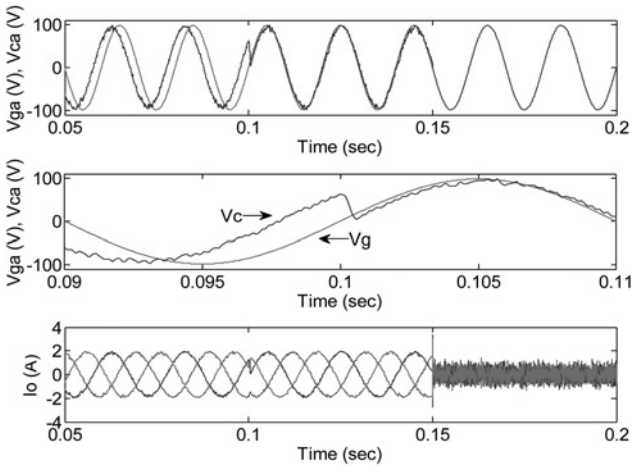

Fig. 8 *Simulation results of grid synchronisation and connection*

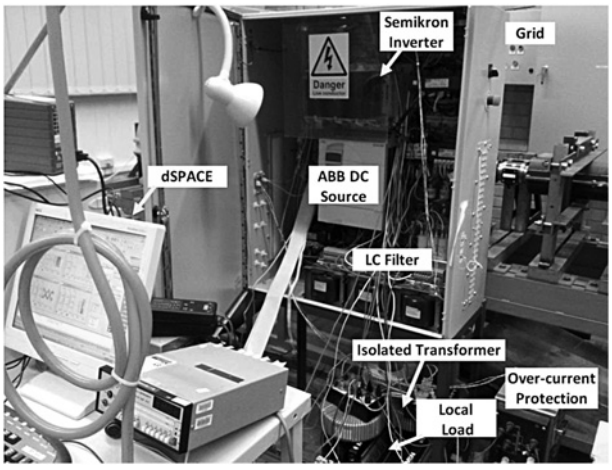

Fig. 10 *Laboratory setup for renewable power generations*

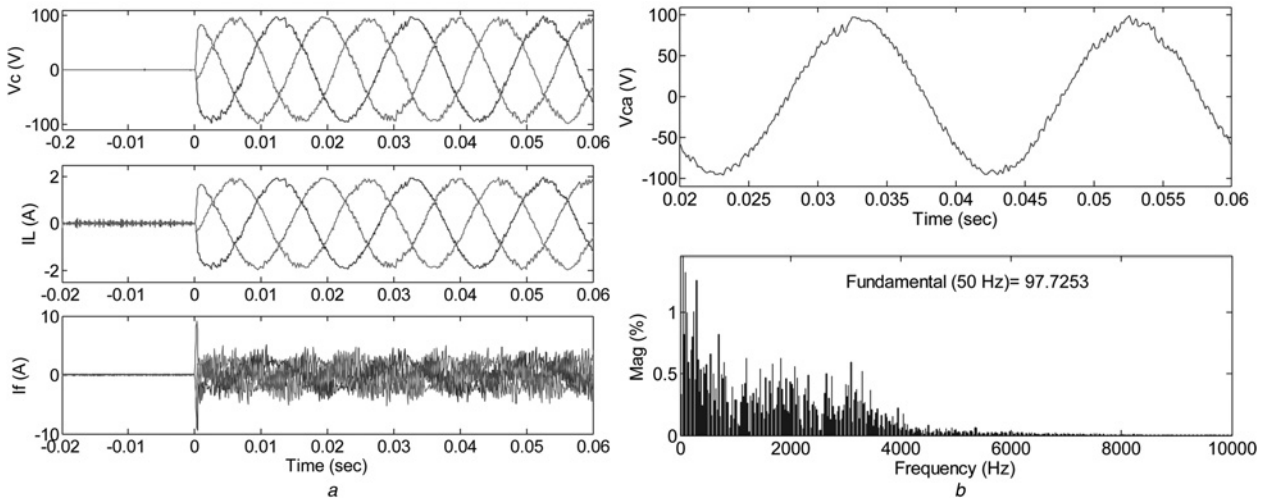

Fig. 11 *Experimental results of islanded operation*

a capacitor voltage, load current, and line inductor current
b spectra of capacitor voltage, THD = 3.70%

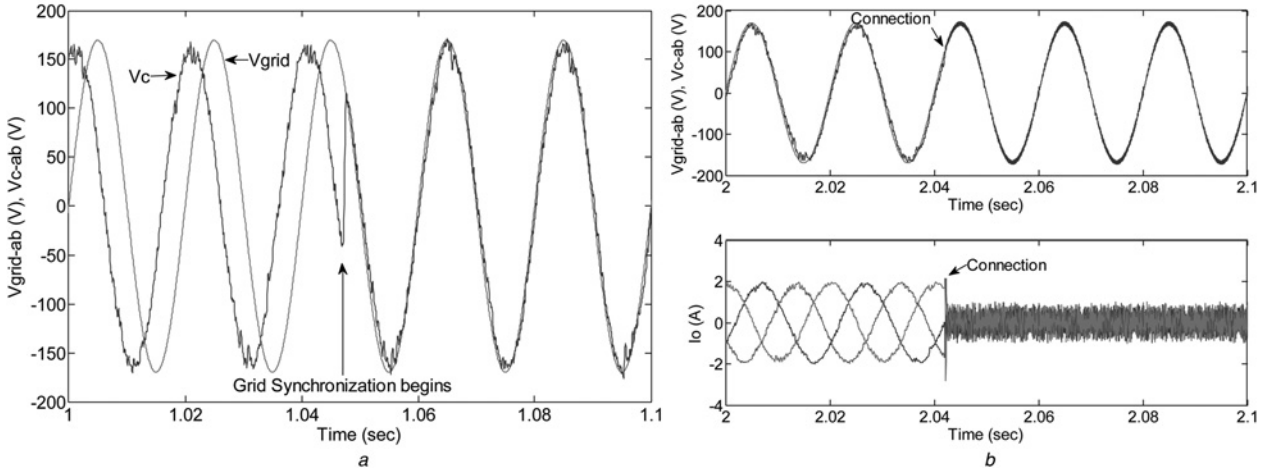

Fig. 12 *Experimental results of grid synchronisation*

a capacitor line-to-line voltage and grid line-to-line voltage during grid synchronisation
b capacitor voltage, grid voltage and inverter output current at grid connection moment

can be seen that the experimental results are in good agreement with the simulation. The capacitor voltage was established quickly and it is very stable. Owing to the resistive load, the load current is proportional to the capacitor voltage. The inductor current presents high-frequency harmonics which are attenuated by the filter. A zoom of the capacitor phase A voltage, V_{ca}, and its spectrum are shown in Fig. 11*b*.

7.2 Grid synchronisation

Fig. 12*a* shows the waveforms of the capacitor and grid voltages. Once the grid synchronisation process begins, the two curves are in close agreement in terms of phase, frequency and magnitude and this is realised very quickly. The grid-connection is then done in a safe and smooth manner by closing S1 and switching off S2, as shown in Fig. 12*b*.

7.3 Grid-connected mode

Once connected to the grid, the bypass switch S_1 is off and the power control algorithm is activated, so the DG system supplies power to the local load and the grid. If the power generated is less than the local load demand, more power would be imported from the grid. On the other hand, if the power generated is larger than the local load demand, the excess will be exported to the grid. Since the conventional STDPC [14, 15] is commonly used it is used here as a benchmark. Fig. 13 shows the dynamic responses of STDPC and the proposed MPC strategy. It can be observed that both the methods present excellent transient performance. However, the power ripples of the proposed strategy are much smaller than that of STDPC, leading to much more sinusoidal line currents. It can be noted that the active and reactive powers shown in Fig. 13 are from the inverter output, not those exchanged between the main grid and the microgrid. For example, the DG system generates -2 kW (-2 kW means power is flowing out from the DG system), the local load consumes $\sqrt{3} \times (120/R_L)^2 = 288$ W, so there are about 1.712 kW of power fed into the grid by the DG system.

In order to validate the effectiveness of the switching frequency reduction of the proposed MPC strategy, a comprehensive set of tests were carried out. These used

doi: 10.1049/iet-rpg.2013.0078

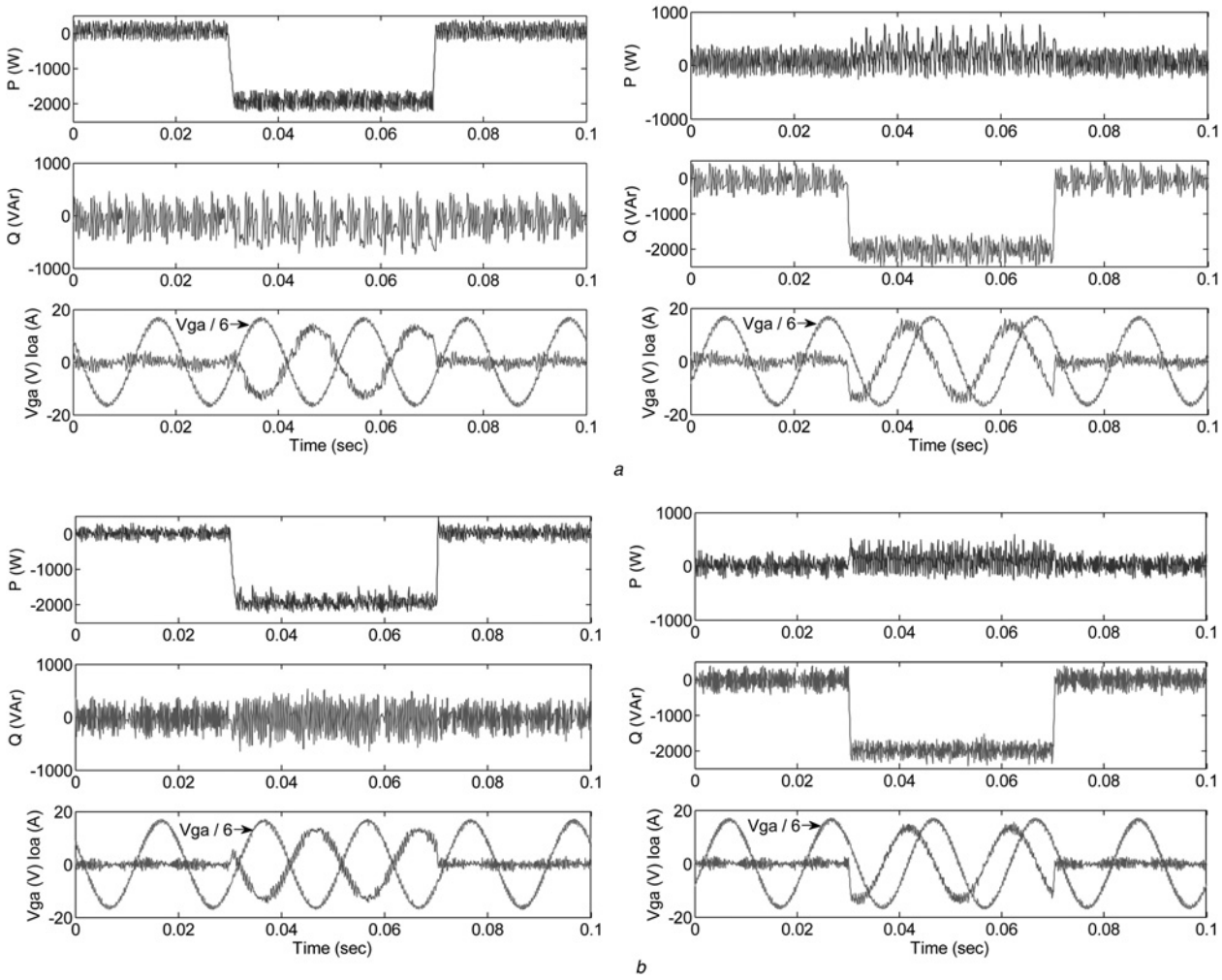

Fig. 13 *Experimental results of flexible power regulation*

a STDPC, left: active power steps, right: reactive power steps
b proposed MPC strategy, left: active power steps, right: reactive power steps

STDPC, the proposed MPC strategy using (27), the proposed MPC strategy using (28) and the proposed MPC strategy using (31). The average switching frequency is calculated by counting the total commutation instances of the PWM gate drive signals of a phase leg were during a fixed period. To obtain a better understanding of the proposed MPC strategy, the quantitative results of the different strategies are summarised in Table 2. It can be seen that the performance of the proposed MPC strategy using (27) is much better than that of STDPC in terms of the power ripple and current THD. This is as expected because the MPC controller selects the most appropriate voltage vector-based on a cost function rather than choosing the vector according to a look-up table. Furthermore, if the switching frequency reduction is also introduced to the cost function, that is using (28), the average switching frequency is reduced considerably to only 968 Hz. However, the system performance deteriorates significantly at this low frequency, with large power ripple and severely distorted inverter output currents with THD = 15.59%. If one further step is made to add a component to (28), that is using (31), the system is stabilised, and the switching frequency is reduced significantly with only slight deterioration in terms of current THD and power ripple compared to the system using (27).

Finally, it is worth mentioning that the optimisation of the weighting factor λ_2 and λ_3 is out of scope of this paper, this specific research topic combined with the knowledge of mathematics and optimisation design is investigated in other research studies such as [22].

Table 2 Quantitative comparison of steady-state performance

Strategy	f_s, Hz	f_{sw}, Hz	THD, %	P_{rip}, W	Q_{rip}, Var
STDPC	20 k	3217	6.35	70.62	105.29
MPC (27)	20 k	3150	2.76	44.55	40.36
MPC (28), $\lambda_2 = 75$	20 k	968	15.59	229.64	132.29
MPC (31), $\lambda_2 = 75$, $\lambda_3 = 0.16$	20 k	1721	3.01	45.38	46.17

(f_s: sampling frequency; f_{sw}: average switching frequency)
(P_{rip}, Q_{rip}: active and reactive power ripples, calculated using standard deviation)

8 Conclusions

This paper proposes a model predictive control strategy for renewable power generation. The proposed control strategy can be used as a general control approach for distributed generation units to achieve islanded operation, grid

synchronisation and grid-connected operation. By changing the cost function appropriately, different control objectives can be fulfilled. In islanded mode, the control objectives are the α and β components of the voltage. In order to achieve grid connection, the voltage reference in the cost function can be replaced by the grid voltage without changing the control structure. After connection to the grid, a new prediction scheme is developed for grid-connected operation, which is a simple and effective way to fulfill flexible active and reactive power regulation. Last but not least, an effective switching frequency reduction algorithm is proposed, which is very attractive in terms of increasing the efficiency of renewable power generation systems.

9 References

1 Maza-Ortega, J.M., Gomez-Exposito, A., Barragan-Villarejo, M., Romero-Ramos, E., Marano-Marcolini, A.: 'Voltage source converter-based topologies to further integrate renewable energy sources in distribution systems', *IET Renew. Power Gener.*, 2012, **6**, (6), pp. 435–445

2 Foster, S., Xu, L., Fox, B.: 'Coordinated reactive power control for facilitating fault ride through of doubly fed induction generator- and fixed speed induction generator-based wind farms', *IET Renew. Power Gener.*, 2010, **4**, (2), pp. 128–138

3 Blaabjerg, F., Liserre, M., Ma, K.: 'Power electronics converters for wind turbine systems', *IEEE Trans. Ind. Appl.*, 2012, **48**, (2), pp. 708–719

4 Blaabjerg, F., Teodorescu, R., Chen, Z., Liserre, M.: 'Overview of control and grid synchronization for distributed power generation', *IEEE Trans. Ind. Electron.*, 2006, **53**, (5), pp. 1398–1409

5 Quinonez-Varela, G., Cruden, A.: 'Modelling and validation of a squirrel cage induction generator wind turbine during connection to the local grid', *IET Gener. Transm. Distrib.*, 2008, **2**, (2), pp. 301–309

6 Wang, F., Duarte, J.L., Hendrix, M.A.M.: 'Grid-interfacing converter systems with enhanced voltage quality for microgrid application – concept and implementation', *IEEE Trans. Power Electron.*, 2011, **26**, (12), pp. 3501–3513

7 Majumder, R., Ghosh, A., Ledwich, G., Zare, F.: 'Load sharing and power quality enhanced operation of a distributed microgrid', *IET Renew. Power Gener.*, 2009, **3**, (2), pp. 109–119

8 Kukrer, O.: 'Deadbeat control of a three-phase inverter with an output LC filter', *IEEE Trans. Power Electron.*, 1996, **11**, (1), pp. 16–23

9 Mattavelli, P.: 'An improved deadbeat control for UPS using disturbance observers', *IEEE Trans. Ind. Electron.*, 2005, **52**, (1), pp. 206–212

10 Marwali, M.N., Keyhani, A.: 'Control of distributed generation systems – Part I: voltage and currents control', *IEEE Trans. Power Electron.*, 2004, **19**, (6), pp. 1541–1550

11 Abdel-Rahim, M., Quaicoe, J.E.: 'Analysis and design of a multiple feedback loop control strategy for single-phase voltage-source UPS inverters', *IEEE Trans. Power Electron.*, 1996, **11**, (4), pp. 532–541

12 Loh, P.C., Newman, M.J., Zmood, D.N., Holmes, D.G.: 'A comparative analysis of multiloop voltage regulation strategies for single and three-phase UPS systems', *IEEE Trans. Ind. Electron.*, 2003, **18**, (5), pp. 1176–1185

13 Cortés, P., Ortiz, G., Yuz, J.I., Rodríguez, J., Vazquez, S., Franquelo, L.G.: 'Model predictive control of an inverter with output LC filter for UPS applications', *IEEE Trans. Ind. Electron.*, 2009, **56**, (6), pp. 1875–1883

14 Noguchi, Tomiki, H., Kondo, S., Takahashi, I.: 'Direct power control of PWM converter without power-source voltage sensors', *IEEE Trans. Ind. Appl.*, 1998, **34**, (3), pp. 473–479

15 Monfared, M., Sanatkar, M., Golestan, S.: 'Direct active and reactive power control of single-phase grid-tie converters', *IET Power Electron.*, 2012, **5**, (8), pp. 1544–1550

16 Alonso-Martinez, J., Eloy-Garcia, J., Arnaltes, S.: 'Table-based direct power control: a critical review for microgrid applications', *IEEE Trans. Power Electron.*, 2010, **25**, (12), pp. 2916–2949

17 Eloy-Garcia, J., Arnaltes, S.: 'Direct power control of voltage source inverters with unbalanced grid voltage', *IET Power Electron.*, 2008, **1**, (3), pp. 395–407

18 Pavlou, K.G., Vasiladiotis, M., Manias, S.N.: 'Constrained model predictive control strategy for single-phase switch-mode rectifiers', *IET Power Electron.*, 2012, (5), pp. 31–40

19 Cortes, P., Rodriguez, J., Antoniewicz, P., Kazmierkowski, M.: 'Direct power control of an AFE using predictive control', *IEEE Power Electron.*, 2008, **23**, (5), pp. 2516–2523

20 Preindl, M., Schaltz, E., Thogersen, P.: 'Switching frequency reduction using model predictive direct current control for high-power voltage sources inverters', *IEEE Trans. Ind. Electron.*, 2011, **58**, (7), pp. 2826–2835

21 Geyer, T., Papafotiou, G., Morari, M.: 'Model predictive direct torque control – Part I: concept, algorithm, and analysis', *IEEE Trans. Ind. Electron.*, 2009, **56**, (6), pp. 1894–1905

22 Thielemans, S., Vyncke, T.J., Melkebeek, J.: 'Weight factor selection for model-based predictive control of a four-level flying-capacitor inverter', *IET. Power Electron.*, 2012, **5**, (3), pp. 323–333

23 Shahabi, M., Haghifam, M.R., Mohamadian, M., Nabavi-Niaki, S.A.: 'Microgrid dynamic performance improvement using a doubly fed induction wind generator', *IEEE Trans. Energy Convers.*, 2009, **24**, (1), pp. 137–145

24 Bojoi, R.I., Limongi, L.R., Roiu, D., Tenconi, A.: 'Enhanced power quality control strategy for single phase inverters in distributed generation systems', *IEEE Trans. Power Electron.*, 2011, **26**, (3), pp. 798–806

doi: 10.1049/iet-rpg.2013.0078